J Therm Anal Calorim (2015) 122:621–633
DOI 10.1007/s10973-015-4813-8

Examining $SrCuO_2$ as an oxygen carrier for chemical looping combustion

E. Ksepko[1]

Received: 17 December 2014 / Accepted: 27 May 2015 / Published online: 23 June 2015

Abstract This paper contains the results of research work on chemical looping combustion (CLC). CLC is one of the most promising combustion technologies and has the main advantage of producing a concentrated CO_2 stream, which is obtained after water condensation without any energy penalty for CO_2 separation. The objective of this work was to study the chemical looping reaction performance for a novel spinel-type oxygen carrier. The $SrCuO_2$ was tested for the purpose of CLC for power generation, and hydrogen was utilized as a syngas component. $SrCuO_2$ was prepared as a powder. Reactivity tests were performed under isothermal conditions for multiple redox cycles using a thermogravimetric (TG) analyzer (Netzsch STA 409 PG Luxx). For the reduction, 3 % H_2 was used, and for the oxidation cycle, air was used. The effect of both reaction temperature (600–800 °C) and reducing/oxidizing cycles (five cycles at each temperature) on the reaction performance of the oxygen carrier samples developed in this study was evaluated. The stability, oxygen transport capacity and reaction rates were analyzed based on experimental TG data. The material was systematically investigated by scanning electron microscopy, X–ray diffraction measurements, N_2 porosimetry, particle size distribution and studying the melting behavior. Investigation of the oxidation/reduction behavior of $SrCuO_2$ showed stable chemical looping performance, with great recyclability after continuous multiple redox reactions maintaining the chemical properties. Moreover, excellent oxygen capacity was maintained within cycling combustion tests. Furthermore, the oxygen carrier sample attained a high melting temperature, which provides attractive thermal resistivity. For comparison purposes, another Cu-based oxygen carrier was prepared and analyzed in the same manner. The CuO/TiO_2 carrier transported similar amounts of oxygen to the fuel, but its stability to reaction was questionable. The promising results obtained from CLC allowed us to conclude that $SrCuO_2$ is possibly a capable and suitable candidate for CLC for power generation.

Keywords $SrCuO_2$ · TG · Hydrogen · Chemical looping combustion · Oxygen transport capacity · XRD

Introduction

In chemical looping combustion, the fuel is converted into pollutant-free energy carriers such as electricity and hydrogen by using an oxygen carrier, typically a metal oxide [1]. An oxygen carrier transfers oxygen from air to fuel as shown in Fig. 1. The two reactors, the reducer and the oxidizer, are also called the fuel and air reactor, respectively. In the fuel reactor, fuel (for example, methane, synthesis gas, coal, biomass) reacts with a solid-state oxygen carrier. In consequence, the fuel is oxidized to CO_2 and H_2O [2], while the metal oxide is reduced to the metal oxide at a lower oxidation state or to its metallic form. After the water condensation, a pure stream of CO_2 in fuel reactor is obtained. Further, in the next step (oxidation of the oxygen carrier), the reduced metal oxide is transferred from fuel reactor to the air reactor where it is regenerated by the air, and then the oxygen carrier is ready to react in another loop with the fuel.

The previous chemical looping combustion studies on materials considered mainly the application of simple

✉ E. Ksepko
eksepko@ichpw.pl

[1] Institute for Chemical Processing of Coal, 1 Zamkowa, Zabrze 41–803, Poland

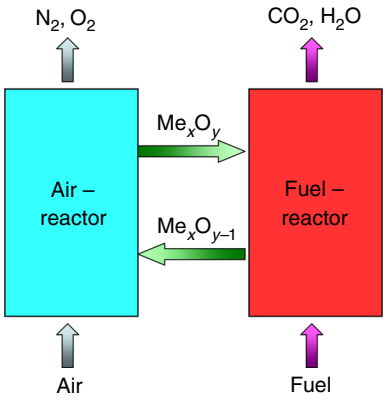

Fig. 1 Chemical looping combustion

synthetic solid oxygen carriers such as NiO, CuO, Fe_2O_3, CoO and MnO_2 [3, 4]. As natural carriers that might be potential candidates for chemical looping, the various ores [5], minerals [6], steel industry wastes [7], sediments from deep water purification [8] and finally sewage sludge ashes [9] were considered, mainly because of their attractive cost contributing to the overall cost of CLC. Recently, synthetic mixed materials have also been investigated intensively due to their emerging CLC properties [10–12]. The complex oxide materials can potentially solve many problems associated with conventional monometallic oxygen carriers [13, 14] because addition of other oxides improves the structural properties of the monometallic oxygen carriers by considerably expanding their stability over multiple redox cycles [15–17]. They have also been proven to increase both the thermal resistance and the oxygen transport capacity [18]. Furthermore, the complex oxide materials improve reaction rates [19–21]. Examples of the complex oxide materials that are receiving considerably increased attention are the spinel system of Cu–Mn–O [17], $CoWO_4$ [22], the MFe_2O_4 type, where *M* is either Co, Ni, Cu, Mg, Ca, Sr or Ba [14], and also perovskite-type materials such as $La_{1-x}Sr_xM_yFe_{1-y}O_{3-\delta}$ [10], or $LaMn_{1-x}Co_xO_{3\pm\delta}$ [23], and $La_{1-x}Sr_xFeO_3$ [20]. In the literature [14], several bimetallic oxygen carriers of the MFe_2O_4 type, where M is either Co, Ni, Cu, Mg, Ca, Sr or Ba and also $MnFeO_3$ were prepared by the precipitation method and were finally tested for potential use in chemical looping combustion of hard coal. Based on collected TG data, bimetallic ferrites were proven to have better reduction rates than the Fe_2O_3 alone. The Group 2 metal ferrites had both better reduction and oxidation rates than transition metal ferrites. $BaFe_2O_4$ demonstrated the highest performance among the bimetallic ferrites studied, and its reduction rate was comparable to the reduction rate of CuO. The cyclic tests on $BaFe_2O_4$ showed stable performance without agglomeration, even at a high temperature of 1000 °C.

The strontium cuprate ($SrCuO_2$) is one of the most interesting materials among other cuprates because it shows high-temperature superconductivity [24, 25]. Some previous studies on the single crystal obtained by the flux method showed that $SrCuO_2$ has a perovskite-like tetragonal structure with an infinite two-dimensional CuO_2 layer structure [25]. $SrCuO_2$ was also recognized as the simplest superconducting compound that showed a transition above the liquid nitrogen temperature [24]. Both atomic position and site occupancy were shown to be closely related to the physical properties. The orthorhombic oxide has a two types of polyhedrons, which form a NaCl-related structure (i.e., there are the Cu–Cu layers made of the distorted NaCl-type structure and also the Cu–Sr and Sr–Sr layers that have the TlI-type structure). Because of the differences in the radii between Sr and Cu, the Cu square plates are distorted from the ideal TlI-type of structure. The calculated copper valence, based on strontium and oxygen occupancy values, showed that the very small portion of copper atoms was monovalent (normalized $Cu^{2+}/Cu^{+} = 0.992/0.008$). Finally, [24] estimated the formula to be $Sr_{0.964}Cu_{0.950}O_{1.914}$, and suggested that the crystals might be slightly doped with electrons.

The brief summary presented here shows that there is an increasing interest in the application of mixed metal oxide oxygen carriers. It is a challenge to find the suitable candidates for the CLC process considering the competing factors such as production cost, availability, stable reactivity during multiple cycles, lower environmental impact than pure Cu or Ni oxygen carriers and the potential impact on human health. Moreover, the oxygen carrier should have a sufficiently high combustion rate as well as an adequate oxygen release capacity to combust the fuel. In addition, a high attrition resistance and a high-temperature resistivity would also be beneficial. The special requirements mentioned are crucial, and they are a must for the practical utilization of oxygen carriers in a chemical looping combustion power plant.

The objective of this paper is the preparation and characterization of mixed metal oxide oxygen carriers that are suitable for chemical looping combustion for power generation (where the hydrogen is the main component of syngas from gasification of coal or biomass). In the present work, $SrCuO_2$ was tested as a potential oxygen carrier for chemical looping processes. The X-ray diffraction (XRD) method for studying the structural properties of the crystal, the high-temperature oven for temperature resistivity and the particle size analyzer for PSD were applied. Fundamentally, the thermogravimetric analysis (TG) was used to determine oxide material redox reactivity with fuel (hydrogen) and ability to transport oxygen and also to determine the stability in cycling redox reactions.

Experimental

Sample preparation

Powder samples of the $SrCuO_2$ were prepared by a mechanical mixing method, by heating the mixture of $SrCO_3$ and CuO oxides (purity 99.9 %) for a total of 20 h at 950 °C. After cooling, the mixture was ground and then calcined at 950 °C for 20 h to ensure the best homogeneity of the oxide material obtained. For comparison purposes, a simple Cu-based oxygen carrier was also prepared. Monometallic 50 mass% CuO, 50 mass% TiO_2 material was prepared by a mechanical mixing method. Molar amounts of CuO and TiO_2 (purity 99.9 %) with the addition of 10 % graphite were calcined in air at 800 °C for 20 h. After cooling and grinding the sample, a new portion of graphite was added to the sample, and then the calcination procedure was repeated under the same conditions.

Basic material characterization

The phase structure and lattice parameters of oxide materials were determined by application of the X-ray powder diffraction (XRD) method. A Siemens D5000 diffractometer with filtered Cu K_α radiation, the $\Theta/2\Theta$ geometry and working parameters such as $V = 40$ kV and $I = 30$ mA was applied. X-ray powder diffraction patterns for polycrystalline samples were recorded at RT in the 2Θ range from 10° to 120°.

The average shrinkage, deformation, hemisphere and flow temperatures were determined by using a high-temperature oven equipped with an IR camera. The pelletized samples were placed in an oven (PR 25/1750/PIE) and heated to 1650 °C to observe the change in the pellet shape during the heating process.

A Malvern Mastersizer 2000 particle analyzer with a dispersion Hydro 2000G mouthpiece was used for the particle size distribution (PSD) analysis. A He–Ne laser with $\lambda = 633$ nm and an LED laser with $\lambda = 466$ nm as the red and blue light source were used.

The scanning electron microscope (SEM) JSM–5410 was used for morphology determination. The SEM was also equipped with an energy dispersion X-ray spectrometer (EDS) with an Si(Li) X-ray detector that was used for investigation of the homogeneity of the samples obtained. Secondary electron images (SEIs) and backscattered electron compositional images (BEI COMPO) were recorded at room temperature for individual grains of the oxygen carrier oxide materials examined.

A Micromeritics 3Flex, that is, an N_2 porosimeter, was used to determine the pore volume and surface area by applying N_2 adsorption isotherms at 77 K. Prior to the measurements, the samples were degassed under vacuum at 350 °C for 4 h. The surface area and pore size were calculated using the Brunauer–Emmett–Teller (BET) and Barrett–Joyner–Halenda (BJH) methods, respectively.

Characterization of reactivity

Thermogravimetric experiments were conducted in a Netzsch STA 409 PG Luxx thermal analyzer that was coupled with a 403C Aëolos quadrupole mass spectrometer (QMS). The mass spectrometer was used for the analysis of the evolved gas and could detect masses between 1 and 300 amu in the SCAN or MID mode. In the TG experiments, the mass change of the metal oxide oxygen carriers was measured isothermally as a function of time. Five reduction/oxidation cycles were performed to determine the reactivity of the oxygen carriers. Approximately 100 mg of sample was heated (with a heating rate of 20 K min^{-1}) in an Al_2O_3 crucible to the reaction temperature. To ensure that the mass transfer limitations during redox reactions were minimal, both the mass of the sample and the flow of the gases were settled experimentally. After reaching the desired temperature, 3 % H_2 balanced by Ar was used for the MeO reduction reaction, while 20 % of the O_2 balanced by N_2 was utilized for the oxidation (regeneration) reaction of the oxygen carrier that had previously been reduced. Because hydrogen is a major component of synthesis gas that might be used for chemical looping combustion for power generation, the possible utilization of a novel Cu-based type of material for this purpose was investigated in this work. Gas flow rates were set at 125 and 50 mL min^{-1}, for reduction and oxidation, respectively. Both reduction and oxidation reaction time was set at 15 min. The TG chamber was flushed with Ar flow for 5 min before and after each redox reaction to avoid the mixing of reduction gases and air. To investigate the effect of temperature, the cyclic tests of reduction–oxidation were carried out over a temperature range of 600–800 °C. Moreover, the complementary, long-term stability performance was also evaluated by investigation of the oxygen carrier within 20 redox cycles at a temperature of 950 °C.

The fractional conversions (fractional reduction and fractional oxidation) were calculated based on collected TG data. The fractional conversion (X) is defined based on observed mass changes within cycling and was calculated using the Eqs. (1) and (2):

$$\text{Fractional reduction}\,(X) = (M_{\text{oxd}} - M)/(M_{\text{oxd}} - M_{\text{red}}) \quad (1)$$

$$\text{Fractional oxidation}\,(X) = (M - M_{\text{red}})/(M_{\text{oxd}} - M_{\text{red}}) \quad (2)$$

where M denotes the instantaneous mass (mass of the metal oxide material), M_{oxd} denotes the mass of a completely

oxidized sample in the TG (completely oxidized oxide in the TG after introducing air) and M_{red} denotes the mass of a completely reduced sample in the TG (the mass of the metal oxide after the reduction reaction). The reaction rates were calculated by differentiating the mass data versus time. The reaction rates shown in this paper are determined as the maximal rates obtained for each separate redox cycle.

Results and discussion

Crystal structure analysis results

Figure 2 shows the X-ray powder diffraction pattern obtained for the $SrCuO_2$ oxygen carrier at room temperature. The determination of the lattice parameters and the phase identification were performed by applying the Rietveld method described elsewhere [26]. Based on the identification of reflections in the X-ray powder diffraction patterns, the cuprate was identified to be an orthorhombic crystal structure. The diffractogram that is shown in Fig. 2 confirmed that $SrCuO_2$ is a single phase. As a result of the fitting of the oxide spectra with utilization of the FullProf program, the $SrCuO_2$ material might be described by the orthorhombic *C mcm* space group, with the following crystal lattice parameters: $a = 3.5713(4)$ Å, $b = 16.3075(5)$ Å, $c = 3.9059(7)$ Å and $V = 227.48$ Å^3. The present results are in good agreement with the earlier studies [24].

Because the mobility of oxygen ions is also expected to be dependent on the distance between ions in the crystal structure [24], the Cu–O distances were calculated. For $SrCuO_2$, the following Cu–O bond lengths are estimated to be 1.891(7), 1.908(0) and 1.955(4) Å × 2 (from the CuO_4 square plate), with an average length of 1.927(6) Å. The numbers given in parenthesis express the significant figures. The three types of Cu–O bonding are present because the crystal structure has two types of cation–polyhedral double layers of SrO_7 and CuO_4 that alternately connect parallel to the direction of the *b* axis, and the stacking along the *c* axis is closely related to the NaCl-like TlI-type structure. The values of the bond lengths differ somewhat slightly from the values obtained from the literature. As reported in [24] for the $SrCuO_2$ monocrystal, the lengths obtained were 1.910(3) Å, 1.930(3) Å and 1.961(4) Å × 2, respectively, with an average Cu–O distance of 1.941(2) Å that was obtained for the oxide with lattice parameters equal to $a = 3.577(1)$ Å, $b = 16.342(1)$ Å and $c = 3.9182(7)$ Å. The Matsushita et al. [24] formula was assumed to be $Sr_{0.964}Cu^{2+}_{0.950}O_{1.91}$. Clearly, the unit cell dimensions obtained in the paper differ from values from the report [24], so therefore the length of the Cu–O bonds has also changed. In the present work, the $SrCuO_2$ material shows shorter Cu–O distances.

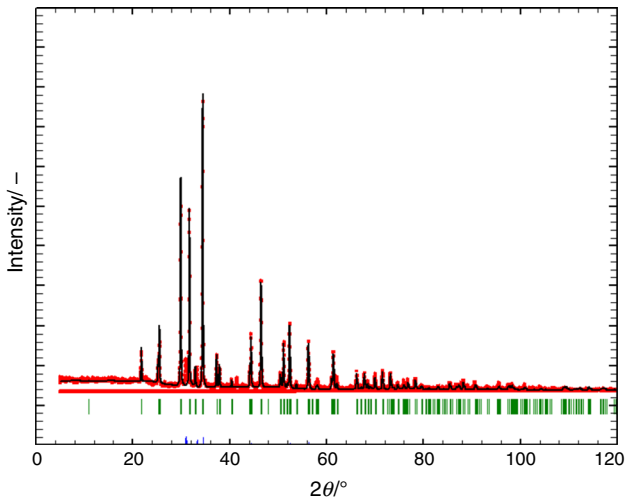

Fig. 2 X-ray powder diffraction pattern collected at room temperature containing the FullProf analysis of crystal structure. Observed (*black line*), calculated (*red line*) profiles for $SrCuO_2$ at RT, refined in the orthorhombic *C mcm* space group. The *vertical markers* correspond to the allowed Bragg reflections

For the oxygen carrier composed of 50 mass% of CuO and 50 mass% of TiO_2, it is the copper oxide (CuO) that is actively taking part in the CLC reactions [27]. For the CuO-based material, the C 2/c space group and the refined crystal lattice parameters were determined as follows: $a = 3.680(3)$ Å, $b = 3.426(5)$ Å, $c = 5.133(1)$ Å, $\beta = 99.4(1)$ and $V = 81.25$ Å^3. The calculated Cu–O bond lengths in CuO are 1.961(2) Å (8 positions) and 1.950(3) Å (4 positions).

Based on the crystal structure data and bond values, we might conclude that the oxygen evolved from the CuO structure will be easier to process than the oxygen evolved from the $SrCuO_2$ material possibly because the longer Cu–O bond lengths that are present for the traditional monometallic oxygen carrier were determined.

Melting behavior study

For solid-state oxygen carriers, the melting points are one of the most important parameters that enable estimation of the agglomeration tendencies because a serious loss of reactivity could appear if the oxygen carrier shows a low melting point. Therefore, the temperature resistance should be high enough both to endure the chemical looping reaction range of temperatures and also to avoid agglomeration of oxygen carrier particles. Usually, the chemical looping processes are operated between 600 °C and 1200 °C [28], and if some metal melts within the said temperature range, the performance of CLC redox reactions could change significantly. Therefore, the average

shrinking, deformation, hemisphere and flow temperatures for $SrCuO_2$ oxygen carrier were determined and are shown in Table 1. The pure chemical used for the oxide synthesis as CuO was tested in terms of thermal resistance. The literature shows that pure CuO has the disadvantage of having a low melting point (1080 °C) [14]. In this work, the deformation of the formed CuO pellet was observed at 630 °C, with melting at 1100 °C, that agrees well with the values reported previously [28]. Therefore, it is important to have some inert additives that may improve the thermal resistivity of the oxygen carrier [28]. Additionally, the melting behavior was tested for the simple supported copper-based (i.e., monometallic CuO/TiO_2) carrier, that is known from [27]. The study showed that adding some inert material may change melting behavior, as is the case known for CuO/TiO_2. Furthermore, the addition of other metal oxides to CuO may improve the thermal resistivity as observed for the advanced $SrCuO_2$ material. That is the case for the $SrCuO_2$ carrier because an increase in temperatures values was obtained for the new $SrCuO_2$ carrier (deformation was observed as high as 1320 °C, while melting was observed at a temperature of 1590 °C). Those temperatures are significantly high compared with the low temperatures of the pure CuO material. Based on results from Table 1, we conclude that a significant improvement of temperature resistivity for strontium cuprate due to the effect of synergy between SrO and CuO oxides was achieved. Moreover, the temperature determined indicated that the material might be used in a CLC system and might operate in the temperature range indicated.

Brunauer–Emmett–Teller (BET) surface area analysis and pore distribution

The surface area and pore analysis data for the oxygen carriers are shown in Table 2. The evaluation of pore size distribution and pore morphology was carried out from the nitrogen sorption isotherms. The $SrCuO_2$ sample showed a low surface area of 1.9 $m^2\ g^{-1}$ as well as a small total volume of the pores equal to 0.0026 $cm^3\ g^{-1}$. For the CuO/TiO_2 carrier, the surface area was 1.3 $m^2\ g^{-1}$, and the total volume of the pores was almost doubled to 0.0043 $cm^3\ g^{-1}$ compared to the $SrCuO_2$ carrier. For both carriers, the surface area was low, with slightly better surface performance observed for strontium cuprate. Based on the N_2 sorption experiments, the volume of micro–, meso– and macropores was determined for both samples (Table 2).

For strontium cuprate, the values were 4.12, 66.70 and 29.18 %, while for copper oxide/titania, the calculated percentage of the micro–, meso– and macropores was 8.52, 55.83 and 35.65 %, respectively. For both samples, the majority of the pores were clearly composed of the mesopores. The cuprate sample is evidently significantly more extended in mesopores compared with the copper oxide/titania oxygen carrier sample. In the copper oxide carrier, the percentage of the micropores is doubled compared to the percentage of cuprate micropores.

The pore morphology was interpreted based on the work of de Boer [29, 30], who envisioned five types of the hysteresis curves and associated the shape of the pores with the form of the hysteresis curves. The geometrical shape of the pore was concluded to be slit-shaped pores (second type of hysteresis curve) for both $SrCuO_2$ and CuO/TiO_2 oxygen carriers. Because the curves of N_2 adsorption isotherms showed that the samples were constructed of slit-shaped pores, the reaction with the gaseous fuel will be easy to carry out because no additional narrows are present Fig. 3. Evolving the oxygen from the oxide materials to the fuel would be favorable for such formed pores. However, based on the data listed in Table 2, we also conclude that the small surface area will not be playing a fundamental role in the reduction–oxidation cycling reactions, but perhaps the pore distribution and pore morphology will be meaningful parameters for the CLC redox reactions.

Particle size distribution (PSD)

PSD data analysis by utilization of the particle size laser analyzer is shown in Fig. 4. The data obtained for $SrCuO_2$ confirmed the particle size to be below 250 μm with the majority of the particle sizes to be 155 μm.

Reactivity study results

Stability of cyclic combustion and regeneration CLC reactions

Because hydrogen is the major compound of synthesis gas (syngas) from the biomass/coal gasification process,

Table 1 Melting points determined for $SrCuO_2$, CuO/TiO_2 and maternal CuO oxide

Sample	Temperature of melting points/°C			
	Shrinking	Deformation	Hemisphere (melting)	Flow
$SrCuO_2$	940	1320	1590	1610
CuO/TiO_2	NA	>1650	>1650	>1650
CuO	630	670	1100	1650

Table 2 BET and pore analysis data for oxygen carriers

Sample	$S_{BET}/m^2\ g^{-1}$	$V_T/cm^3\ g^{-1}$	$V_{micro}/cm^3\ g^{-1}$	$V_{meso}/cm^3\ g^{-1}$	$V_{macro}/cm^3\ g^{-1}$
$SrCuO_2$	1.9	0.0026	0.0001	0.0017	0.0008
CuO/TiO_2	1.3	0.0043	0.0004	0.0024	0.0015

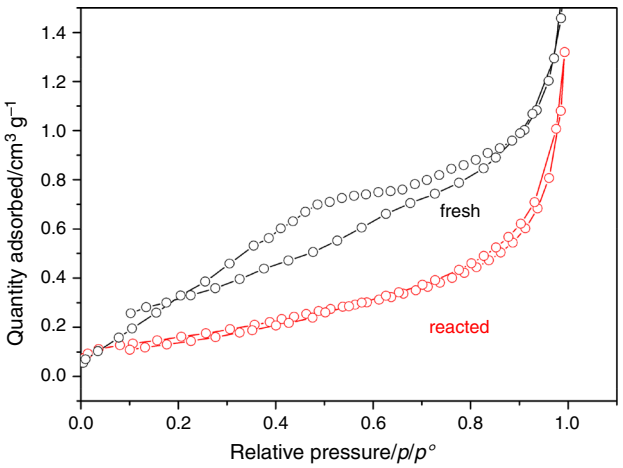

Fig. 3 N_2 adsorption isotherms for both fresh and reacted $SrCuO_2$ samples

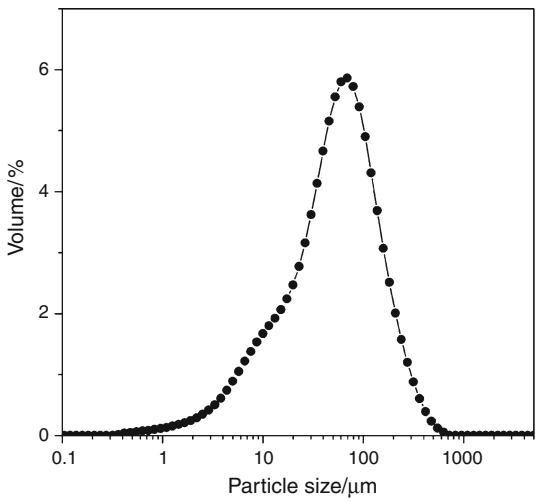

Fig. 4 Particle size distribution

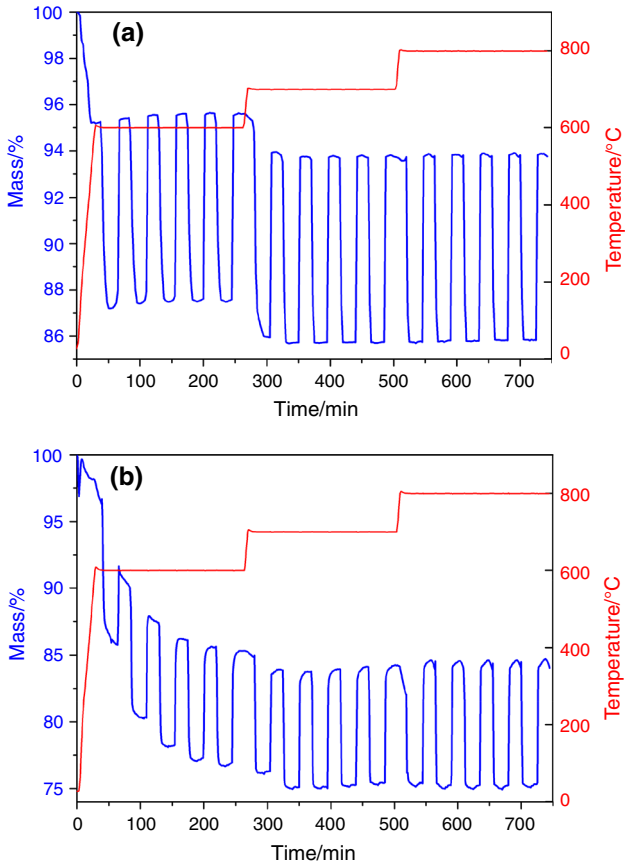

Fig. 5 Five-cycle reduction/oxidation TG data for **a** $SrCuO_2$, **b** CuO/TiO_2 at 600–800 °C

hydrogen was therefore utilized as a fuel in CLC testing [1, 2]. Five cycles of reduction–oxidation TG data were obtained for the $SrCuO_2$ oxygen carrier at the 600–800 °C temperature range, shown in Fig. 5a. The stable reaction performance was observed for the oxygen carrier within the studied temperature range, while 3 % H_2 was used as a reducing agent. Some mass decrease observed at the beginning of the cycling CLC reactions (approximately 5 min) that may be attributed to the water content. That observation was supported by the mass spectrometer (MS) data that confirmed the presence of the H_2O peak within the maximum rate observed at the 109 °C temperature.

Figure 5b shows the five-cycle reduction/oxidation TG data for monometallic oxygen carrier CuO/TiO_2 that was collected at 600–800 °C. Similarly, at the beginning of the cycling tests, a similar behavior was observed for $SrCuO_2$, i.e., the mass loss due to the presence of the water content. Then, the sample was reduced and oxidized in a cycle. However, at 600 °C, the decrease in mass shows that the sample must be activated at least within four redox cycles. At a temperature of 700 °C, the cycling performance shows that for achievement of cycling stability, at least two redox cycles must be carried out. Further heating to the 800 °C temperature causes the CuO/TiO_2 oxygen carrier to demonstrate the repeatable redox cycling performance. Based on the data shown in Fig. 5a, b, we may conclude

that the $SrCuO_2$ compound shows better performance than the typical monometallic oxygen carrier of CuO/TiO_2 because $SrCuO_2$ oxide did not need an activation period for operating at 700 and 800 °C.

Because one of the most important factors for selection of a solid-state oxygen carrier for CLC application is the ability to transport oxygen to the fuel, an oxygen transport capacity for both the new $SrCuO_2$ and CuO/TiO_2 based on TG data was estimated. The capacities were calculated for each single cycle of reduction–oxidation TG data recorded for 600, 700 and 800 °C temperatures, and the capacities are shown in Fig. 6a, b. The capacity stability for the $SrCuO_2$ oxygen carrier versus the cycle number showed stable performance at all temperatures studied. At a temperature of 600 °C, a high capacity of 7.97 mass% was estimated for the first cycle, then the capacity increased slightly with an increase in the cycle number. For the third cycle, a mass% capacity of 8.07 was estimated, then the capacity was stabilized at level of 8.02 %. A similar behavior was observed for 700 °C, i.e., a small increase in capacity and finally the smooth stabilization, while for 800 °C, a slight decrease at the beginning and then stabilization. That behavior might be due to reorganization of the pore structure during reduction–oxidation cycling because the pore structure was possibly changed with the number of cycling reactions.

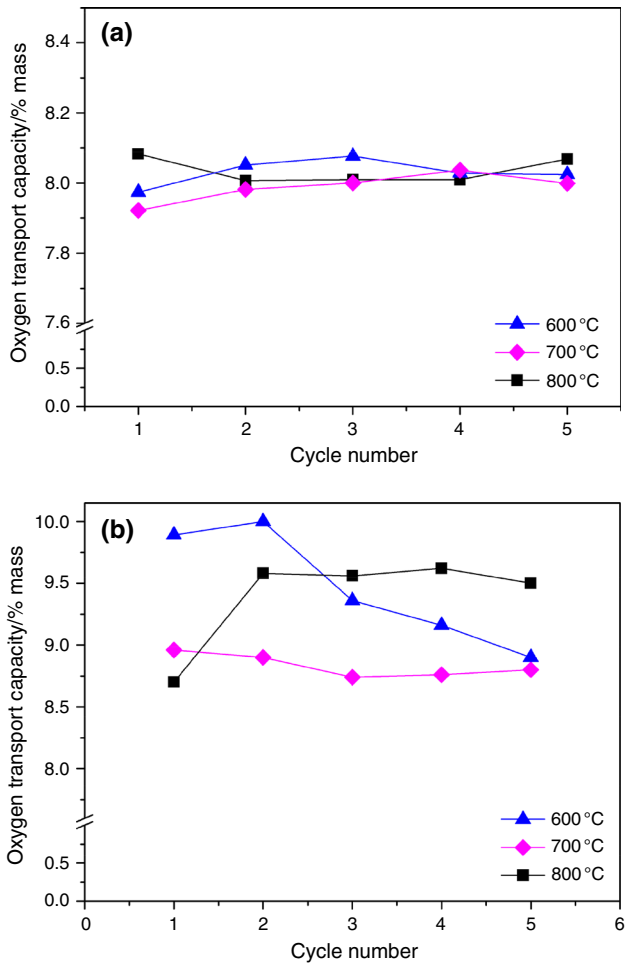

Fig. 6 Oxygen transport capacity for oxygen carriers versus cycle number for (a) $SrCuO_2$ and (b) CuO/TiO_2 at 600 °C, 700 °C and 800 °C

To support this hypothesis, the BET and pore analysis for reacted samples was completed (Fig. 3). The samples reacting for five redox cycles at 800 °C showed a surface area of 0.59 $m^2\ g^{-1}$ that is low compared to the fresh surface area of 1.91 $m^2\ g^{-1}$. While cycling, the surface area has decreased. Nevertheless, the volume of micro–, meso– and macropores remained almost the same (0.0001, 0.0011 and 0.0008 $cm^3\ g^{-1}$). Moreover, based on the pore distribution data, we may conclude that the ratio of pores has changed in favor of the macropores because for the reacted sample 6.41, 54.21 and 39.38 % for micro–, meso– and macropores was assumed, while for the fresh sample, a calculated percentage of 4.12, 66.70 and 29.18 % for micro–, meso– and macropores was observed. The surface area of reduced samples significantly decreased after five-cycle test as showed from N_2 adsorption measurements, while volume of micro-, meso- and macropores remained almost the same. The reason for that is that mean pore diameter calculated on the basis of BET has changed from 2.2735 to 8.8875 Å for fresh and reacted sample, respectively. In other words, three times higher pore diameter was produced in the reacted samples, while three times lower surface area was observed. Furthermore, the total pore volume (V_T) in the fresh sample was higher and was equal to 0.0026 $cm^3\ g^{-1}$ comparing to the total pore volume value of 0.0020 $cm^3\ g^{-1}$ for reacted sample. In other words, the increase in pore volume and in mean pore diameter contributed to the decrease of surface area of reacted OC samples.

Further heating of the sample to a temperature of 800 °C caused a small increase in oxygen carrying capacity with a maximum capacity of 8.08 mass% observed for the first cycle, then the oxygen carrying capacity decreased and stabilized smoothly at 8.00 mass% at the end of the cycling reactions. Based on the data presented, a negligible temperature effect on the oxygen release was observed for the $SrCuO_2$ carrier in the 600–800 °C temperature range. For the $SrCuO_2$ carrier, even a reaction temperature as low as 600 °C with gaseous fuel might be applied for low-temperature CLC.

The theoretical maximum extent of mass reduction that was calculated for the $SrCuO_2$ oxygen carrier was equal to 17.47 mass% when evolving whole oxygen (2 mol) that is available in the chemical looping combustion reaction. For reduction in the oxide with release of 1 mol of oxygen, the theoretical extent of reduction would be equal to 8.74 mass%. At 800 °C, the maximum extent of reduction

that was observed based on TG data showed that the experimental value was estimated at 8.08 mass% for the $SrCuO_2$ carrier. Therefore, the observed mass changes might be expressed as reversible reduction–oxidation reactions based on the following formula:

$$SrCuO_2 \underset{ox.}{\overset{red.}{\leftrightarrow}} SrCuO_{1.075} + 0.462\,O_2$$

For the CuO/TiO_2 oxygen carrier, the calculated capacity stability within the cycle number differs significantly from the value observed for $SrCuO_2$ that is shown in Fig. 6b. At the lowest temperature and at the first cycle, the sample showed a high oxygen capacity of 9.89 mass%, then the oxygen capacity decreased with an increase in the cycle number. Therefore, at the fifth cycle, the sample showed the lower 8.9 mass% capacity. That value might be observed due to difficulties with releasing the oxygen and possible agglomeration of the particles. For 700 °C at the beginning of cycling, the sample shows a lower capacity (8.96 mass%) than the capacity observed at 600 °C, and the capacity also decreased with an increase in the cycle number. However, the decrease was smaller than the decrease at 600 °C. At 800 °C, an intermediate capacity was observed. At the first cycle, the capacity was 8.7 mass%. Then, the capacity increased considerably for the second cycle and stabilized at approximately 9.6 mass% (cycles 2–5). That behavior means the temperature had some positive effect on oxygen capacity. In general, the higher the temperature, the higher the capacity that may be achieved. However, serious concerns might arise due to a possible tendency for agglomeration that may be concluded from the results shown.

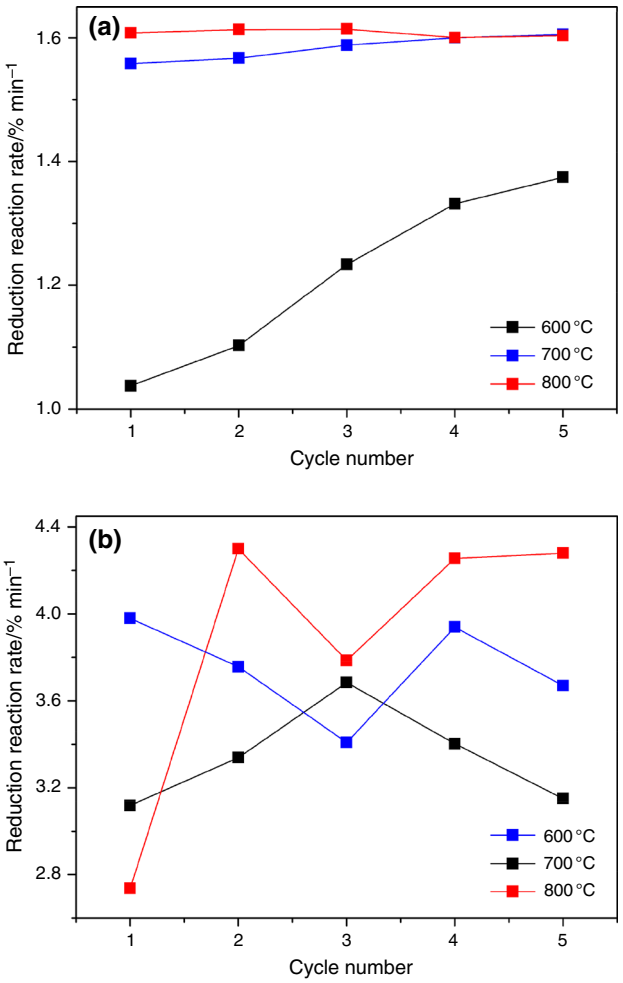

Fig. 7 Reduction reaction rate for oxygen carriers versus cycle number at given temperatures for **a** $SrCuO_2$, and **b** CuO/TiO_2

Reduction reaction performance

The reactivity of the oxygen carrier was evaluated on the basis of TG data obtained from the cycling redox reaction. The calculated reaction rates that are shown as reaction rates at the maximum of the peak, both for reduction and oxidation reactions, are shown in Figs. 7 and 8, respectively.

Figure 7a shows that the reduction reaction rate increased with the increase in cycle number for $SrCuO_2$ at 600 °C, but for 700 °C, and 800 °C, the reduction reaction rate was stable because at 600 °C, the increase in reduction rate is significant. For the first reduction cycle, the assumed rate was equal to 1.03 % min^{-1}, and for the fifth cycle, the assumed rate was equal to 1.37 % min^{-1}. A continuous increase in reduction reaction rate was observed with the increase in cycling number at 600 °C. That increase in rates might be due to the reorganization of crystal structure and pore reorganization (increase in size) that was supported by SEM microphotographs. The increase might possibly be the reason that the oxygen ions were easily removed from the cuprate structure.

As the temperature increased, the reduction rate also increased to approximately 50 %, the case for 700 °C. The further heating of the sample (up to 800 °C) resulted in a further increase in reduction reaction rate. However, the increase in rates is minor compared to the increase in rates observed between the temperatures of 600 and 700 °C. At the highest temperature (800 °C), the maximum rate was 1.60 % min^{-1}. The temperature was observed to have a positive effect on the reduction reaction rates: the higher the temperature, the faster the hydrogen combustion rates that were observed. The temperature facilitates the reduction in the oxygen carrier by hydrogen.

In Fig. 7b, the reduction reaction rates for CuO/TiO_2 oxygen carriers versus cycle number at particular temperatures are given. The calculated rate changes do not show a definite tendency and are much different from the behavior that was observed for cuprate because at 600 °C, the

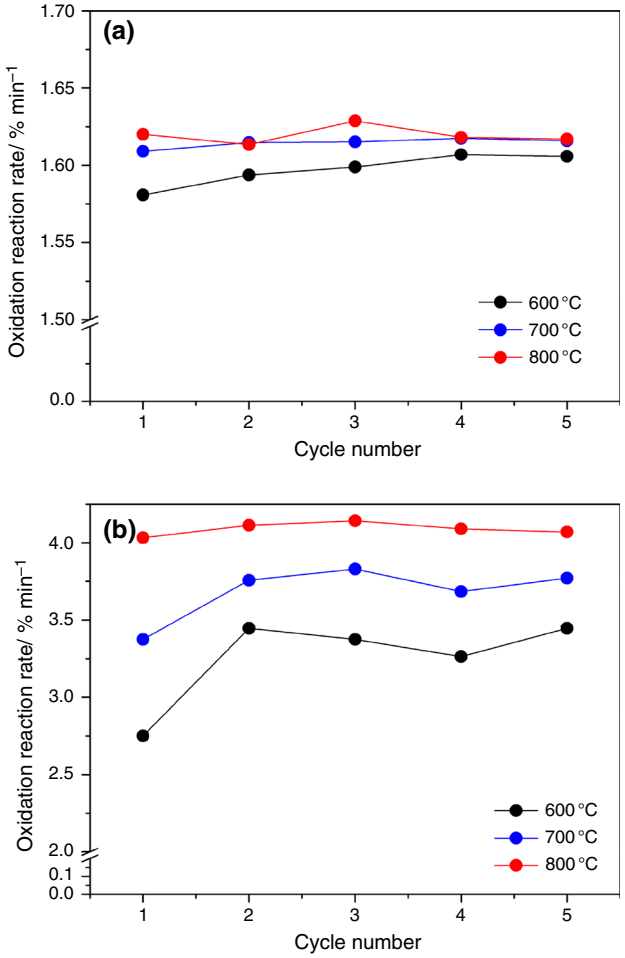

Fig. 8 Oxidation reaction rate for oxygen carriers versus cycle number at given temperatures for **a** $SrCuO_2$, and **b** CuO/TiO_2

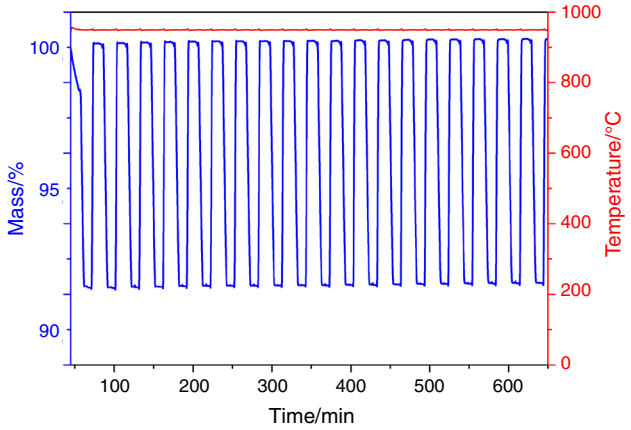

Fig. 9 Results of long cycling CLC testing: TG data at 950 °C

highest reduction reaction rate (3.97971 % min^{-1}) was observed for the first cycle, then the reduction reaction rate decreased with an increase in the cycle number up to the third cycle, then the reduction reaction rate increased and decreased again for the fifth cycle. That behavior is in contrast with the behavior observed at higher temperatures because the heating of the sample up to a temperature of 700 °C leads to lower reduction rates than heating the sample to 600 °C. At the beginning of the cycling, the 3.11884 % min^{-1} rate was estimated, with an increase in rate up to the third reduction cycle, and finally, a significant drop-off in rates was observed. For the highest temperature (800 °C), the estimated rate of 2.73623 % min^{-1} was observed at the beginning of the CLC reduction reaction (first cycle), then the intensive increase in rate, decrease and increase again for the fourth and fifth cycles and finally the stabilization of the rate at a level of 4.27826 % min^{-1} (fifth cycle). Therefore, in contrast to $SrCuO_2$, for CuO/TiO_2, no general rules for the effect of temperature on reaction rates were observed. The decrease in rates with cycle number might be explained by the fact that even at a temperature as low as 600 °C, CuO is reduced to metallic Cu. This conclusion is based on the theoretical oxygen capacity that should have been approximately 10.05 mass% and agree well with the experimental data. Based on that conclusion and because metallic Cu particles are known from literature to possess an agglomeration tendency, causing difficulty in allowing H_2 to penetrate through CuO particles, some reduction reaction rates were therefore observed to decrease.

Based on the calculated reduction rate values, CuO/TiO_2 clearly reduces faster than $SrCuO_2$ because the estimated rate ratio was equal to 1.96–2.67. However, the reduction stability of the monometallic Cu-based carrier (at 600–800 °C) is obviously poor, making the material less predictable as an oxygen carrier material for the CLC process. For practical application as an oxygen carrier, a sufficient stability of reactivity should be provided while more suitable candidate material is selected. Based on our data for the comparison of the stability of the new $SrCuO_2$ and standard monometallic CuO/TiO_2, carriers were tested under identical conditions. Standard monometallic CuO/TiO_2 showed dramatically unstable performance across the redox cycle numbers. The involvement of Sr, Cu and O may result in a better redox CLC stability than the involvement of Ti, Cu and O obtained for the simple monometallic Cu-based oxygen carrier.

Regeneration ability

The oxidation (regeneration) reaction rates as a function of the cycle number for a given temperature are shown in Fig. 8a–b. The rates were calculated to evaluate the oxidation ability of the materials. A similar behavior was observed for regeneration reactions such as the reaction for the reduction in the oxygen carrier material because the regeneration reaction rate for the $SrCuO_2$ sample increased

both with cycle number and also with an increase in temperature. The 1.58073–1.62878 % min^{-1} oxidation rate that was estimated is similar to the oxidation rate that was estimated for reduction reaction. The stabilization of rates was also observed for the fourth cycle, similar to the stabilization for reduction reaction rates. The rates have systematically and smoothly increased with temperature; therefore, the effect of temperature on the oxidation rates was positive. However, the magnitude of the effect was much smaller than the magnitude of the effect for the reduction reaction. As shown in Fig. 8a, the $SrCuO_2$ regenerated smoothly and its regeneration performance was excellent.

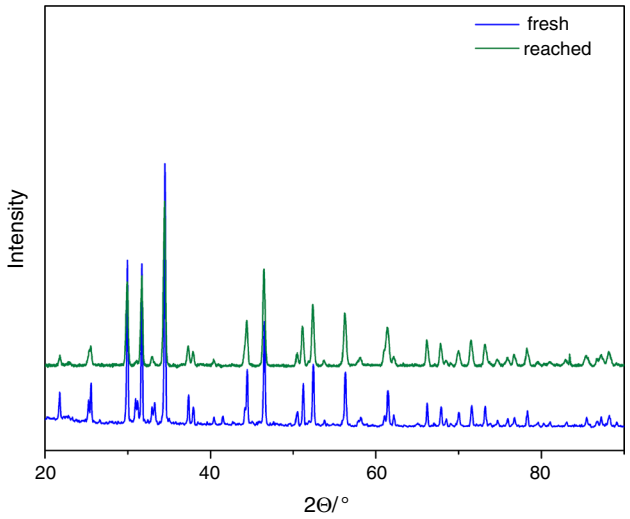

Fig. 10 Comparison of XRD pattern between fresh and reacted samples

For CuO/TiO_2, the regeneration data (Fig. 8b) show both the effect of the cycle number and the effect of temperature on regeneration performance. The oxidation rates are high, and an increase in rate between cycles 1 and 2 is observed, then the rates were stabilizing. The effect of temperature on rates is positive because the rates were 3.44638, 3.77101 and 4.06957 % min^{-1} for 600, 700 and 800 °C temperature, respectively. The oxidation reaction rates are higher for an increase in 2.15–2.49 compared to strontium cuprate oxidation rates.

The $SrCuO_2$ oxide sample was also examined in terms of long cyclic performance at 950 °C. Twenty redox cycles of TG data with hydrogen as the fuel (3 % H_2/Ar) are shown in Fig. 9. The oxygen carrier sample showed an excellent performance because the mass changes remained the same within the long-term study with temperatures as high as 950 °C. The utilization of oxygen was maintained at approximately 8–9 % during 20 cycles. Continuous redox cycles operating at 950 °C temperature indicated that the cuprate exhibited excellent steady recyclability. That means that the proposed cuprate material might be a valuable tool for chemical looping combustion reactions as an oxygen carrier.

To evaluate the regeneration ability of the oxygen carrier, both the morphology of the sample by SEM and phase

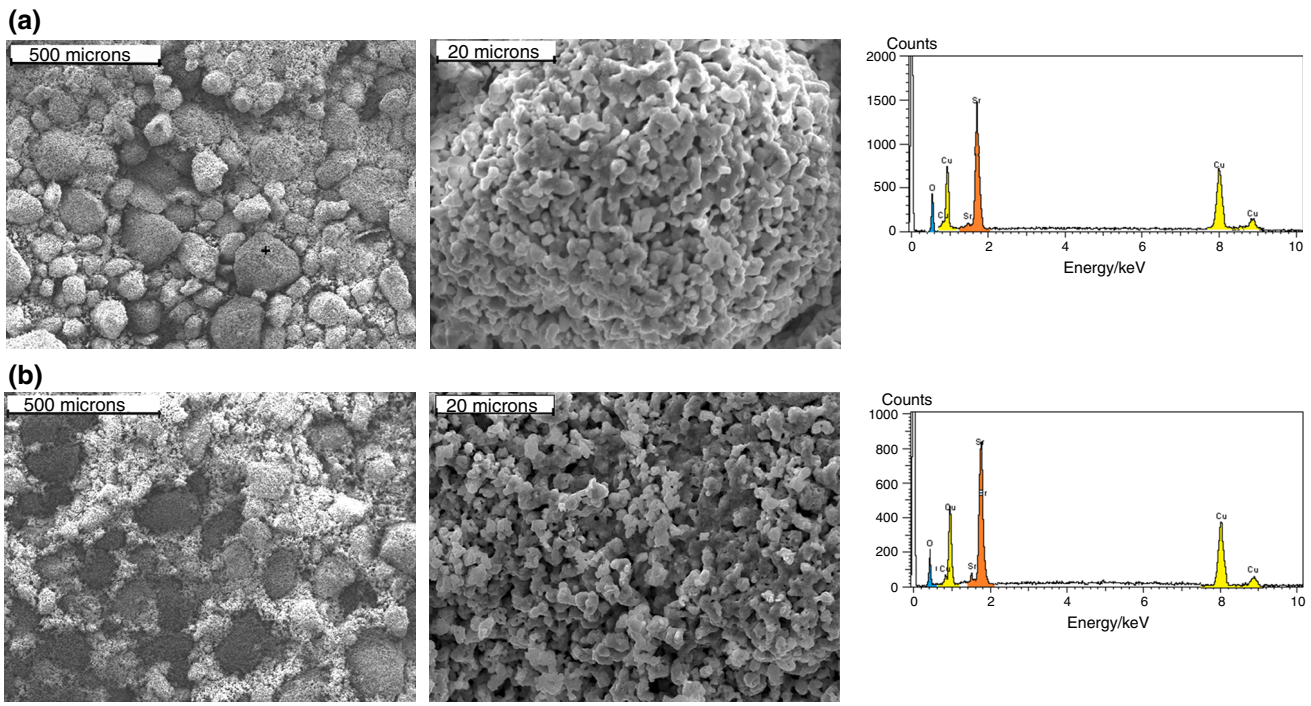

Fig. 11 SEM photomicrographs and EDX analysis for **a** fresh and **b** regenerated $SrCuO_2$ sample

composition analysis by XRD were carried out. The X-ray powder diffraction pattern for both unreacted and reacted samples (20 cycles) is shown in Fig. 10. The figure shows that the regenerated sample did not demonstrate the substantial crystal phase changes due to cycle redox tests. The better stability of $SrCuO_2$ with fuel, compared to the stability of CuO/TiO_2, could be due mainly to crystal structure differences as described previously. Because the phase composition remained the same, $SrCuO_2$ might be a potential candidate for an oxygen carrier due to its high stability performance and efficient regeneration ability.

The surfaces of fresh and reacted samples were observed by SEM to note if the sample had undergone any morphological changes after multiple reduction and oxidation cycles. Figure 11a–b illustrates the SEM microphotographs of fresh and cycled $SrCuO_2$ samples, respectively. The SEM images of the surface of the samples were taken at different magnifications (100× and 2000×). The fresh and reacted samples showed a granular structure with particles 100–250 μm in length. At 2000× magnification, the samples are fine powders with each sub-grain structured, the case for both fresh and reacted samples. Both SEM and XRD data confirmed the phase purity. The quasi-spherical grains of approximately 1–5 μm and small pores were observed for both fresh and reacted samples. However, the SEM images of the surface of the carriers did not show any additional formation of the other phases after cycling tests. Based on Fig. 11a–b, no melting or agglomeration tendency was observed for the developed material. The material that was developed did not demonstrate noticeable change compared to fresh carrier as revealed in Fig. 11. However, the small increase in porosity was observed due to cycling reactions as shown in Fig. 11b. We conclude that the microstructure of the oxygen carrier samples was stable in the course of the cyclic reactions because the SEM did not indicate that the samples either undergo a shape evolution or even develop into different morphologies, as shown in Fig. 11b.

The EDX analysis confirmed the stable performance of the oxygen carrier samples because the chemical composition did not change after redox reaction cycles.

In summary, the strontium cuprate carrier showed the outstanding stable reactivity (maximum of 20 cycles at 950 °C) that was observed for all of the measured temperatures. $SrCuO_2$ therefore appears to be a repeatable and stable oxygen carrier material proven for a temperature range of 600–950 °C.

Conclusions

In this study, new Cu-based material suitable for the chemical looping processes was developed. The redox properties of the $SrCuO_2$ (strontium cuprate) have been characterized for CLC and have been reported for the first time. Moreover, there is no information in the literature regarding this particular material for application to chemical looping combustion. In the present work, an emphasis was placed on a possible practical application of $SrCuO_2$ for power generation.

The oxygen carrier showed stable performance during the five-cycle TG tests at temperatures of 600–800 °C, while at 950 °C, the length of the 20 redox cycle test that was performed proved its stability. The oxygen transport capacity that was determined is the important factor for the chemical looping processes that were calculated from the TG data. The effect of the temperature on the oxygen transport capacity was also determined. At 600 °C, the oxygen capacity for the fifth redox cycle was determined to be 8.02 mass% for the $SrCuO_2$ oxygen carrier. With an increase in temperature (200 °C), only a negligible increase in oxygen capacity was observed because at 800 °C, the oxygen capacity was estimated to be 8.08 mass%. The $SrCuO_2$ oxygen carrier was able to release oxygen as a temperature as low as at 600 °C, as our data support. The TG data also indicated that $SrCuO_2$ showed both ability to react with the fuel and the ability to react with air. The effect of temperature on the reactivity of the materials was also determined because the reaction rates increased with an increase in temperature.

The advantage of the material was good reactivity with hydrogen as a fuel (a part of the synthesis gas from the coal/biomass gasification process) that might be promising for the power generation process. Moreover, reduction and regeneration reactions were fast and showed repeatable performance with CLC redox cycle number. The strontium cuprate material showed that strontium cuprate might also be reversibly regenerated, maintaining the physical–chemical properties (as also supported by SEM data). The multi-cyclic redox reaction results indicated that the synthesized oxide oxygen carriers have good regeneration ability, which is a very important parameter that is required in chemical looping combustion applications. The phase composition for oxygen carriers also did not change in cycling combustion of hydrogen and oxidation by air reactions. High melting temperatures that were determined to be as high as 1590 °C showed no signs of agglomeration, resulting in high-temperature stability over multiple redox cycles with 3 % H_2. In this study, other Cu-based carriers were investigated for comparison purposes. The monometallic CuO/TiO_2 carrier transported similar amounts of oxygen to the fuel, as indicated by TG measurements. However, detailed study showed that the CLC performance stability of the monometallic CuO/TiO_2 carrier was poor. Systematic investigations using TG, SEM and XRD methods showed superior behavior of cuprate over the classical monometallic carrier. Even if both

compounds contained roughly similar amounts of Cu (ca. 35 mass%), they also transported roughly similar amounts of O_2 (approximately 8 mass%). $SrCuO_2$ showed excellent stable and predictable performance for the successive redox cycles by maintaining activity and durability. No deactivation with cycle number or increased temperature was observed.

A deeper approach toward the redox properties of strontium cuprate was carried out in the present study, and the results obtained demonstrated the feasibility of using the material as an oxygen carrier in a chemical looping application.

Acknowledgements The research leading to these results has received funding from the People Programme (Marie Curie Actions) of the European Union's Seventh Framework Programme FP7/2007–2013/under REA grant agreement n° PIRSES–GA–2013–612699 entitled "Long-term research activities in the area of advanced CO_2 capture technologies for Clean Coal Energy Generation—"CO2TRIP and was also partially funded by the Polish Ministry of Higher Education and Science, Decision No. 3111/7.PR/2014/2 as "Scientific work financed from the funds for science in years 2014–2017, allocated for completion of the international co-financed project".

References

1. Cleeton JPE, Bohn CD, Müller CR, Dennis JS, Scott SA. Clean hydrogen production and electricity from coal via chemical looping: identifying a suitable operating regime. Int J Hydrogen Energy. 2009;34(1):1–12. doi:10.1016/j.ijhydene.2008.08.069.
2. Chen S, Shi Q, Xue Z, Sun X, Xiang W. Experimental investigation of chemical-looping hydrogen generation using Al2O3 or TiO2-supported iron oxides in a batch fluidized bed. Int J Hydrogen Energy. 2011;36(15):8915–26. doi:10.1016/j.ijhydene.2011.04.204.
3. Eyring EM, Konya G, Lighty JS, Sahir AH, Sarofim AF, Whitty K. Chemical looping with copper oxide as carrier and coal as fuel. Oil Gas Sci Technol-Rev IFP Energies Nouv. 2011;66(2):209–21.
4. Adánez J, de Diego LF, García-Labiano F, Gayán P, Abad A, Palacios JM. Selection of oxygen carriers for chemical-looping combustion. Energy Fuels. 2004;18(2):371–7. doi:10.1021/ef0301452.
5. Tian H, Siriwardane R, Simonyi T, Poston J. Natural ores as oxygen carriers in chemical looping combustion. Energy Fuels. 2013;27(8):4108–18. doi:10.1021/ef301486n.
6. den Hoed P, Luckos A. Oxidation and reduction of iron-titanium oxides in chemical looping combustion: a phase-chemical description. Oil Gas Sci Technol-Rev IFP Energies Nouv. 2011;66(2):249–63.
7. Jerndal E, Leion H, Axelsson L, Ekvall T, Hedberg M, Johansson K, et al. Using low-cost iron-based materials as oxygen carriers for chemical looping combustion. Oil Gas Sci Technol-Rev IFP Energies Nouv. 2011;66(2):235–48.
8. Ksepko E. Feasible utility of inorganic remains from potable water purification process in chemical looping combustion studied in TG. J Therm Anal Calorim. 2014;120(1):457–70. doi:10.1007/s10973-014-3973-2.
9. Ksepko E. Sewage sludge ash as an alternative low-cost oxygen carrier for chemical looping combustion. J Therm Anal Calorim. 2014;116(3):1395–407. doi:10.1007/s10973-013-3564-7.
10. Nalbandian L, Evdou A, Zaspalis V. $La_{1-x}Sr_xMyFe_{1-y}O_{3-\delta}$ perovskites as oxygen-carrier materials for chemical-looping reforming. Int J Hydrogen Energy. 2011;36(11):6657–70. doi:10.1016/j.ijhydene.2011.02.146.
11. Evdou A, Zaspalis V, Nalbandian L. $La_{1-x}Sr_xFeO_{3-\delta}$ perovskites as redox materials for application in a membrane reactor for simultaneous production of pure hydrogen and synthesis gas. Fuel. 2010;89(6):1265–73. doi:10.1016/j.fuel.2009.09.028.
12. Wang B, Xiao G, Song X, Zhao H, Zheng C. Chemical looping combustion of high-sulfur coal with NiFe2O4-combined oxygen carrier. J Therm Anal Calorim. 2014;118(3):1593–602. doi:10.1007/s10973-014-4074-y.
13. Ksepko E, Sciazko M, Babinski P. Studies on the redox reaction kinetics of Fe2O3–CuO/Al2O3 and Fe2O3/TiO2 oxygen carriers. Appl Energy. 2014;115:374–83. doi:10.1016/j.apenergy.2013.10.064.
14. Fan Y, Siriwardane R. Novel new oxygen carriers for chemical looping combustion of solid fuels. Energy Fuels. 2014;28(3):2248–57. doi:10.1021/ef402528g.
15. Rydén M, Lyngfelt A, Mattisson T, Chen D, Holmen A, Bjørgum E. Novel oxygen-carrier materials for chemical-looping combustion and chemical-looping reforming; $La_xSr_{1-x}Fe_yCo_{1-y}O_{3-\delta}$ perovskites and mixed-metal oxides of NiO, Fe2O3 and Mn3O4. Int J Greenh Gas Control. 2008;2(1):21–36. doi:10.1016/S1750-5836(07)00107-7.
16. Ksepko E, Łabojko G. Effective direct chemical looping coal combustion with bi-metallic Fe–Cu oxygen carriers studied using TG–MS techniques. J Therm Anal Calorim. 2014;117(1):151–62. doi:10.1007/s10973-014-3674-x.
17. Azad A-M, Hedayati A, Rydén M, Leion H, Mattisson T. Examining the Cu–Mn–O spinel system as an oxygen carrier in chemical looping combustion. Energy Technol. 2013;1(1):59–69. doi:10.1002/ente.201200009.
18. Zhu X, Wei Y, Wang H, Li K. Ce–Fe oxygen carriers for chemical-looping steam methane reforming. Int J Hydrogen Energy. 2013;38(11):4492–501. doi:10.1016/j.ijhydene.2013.01.115.
19. Ku Y, Liu Y-C, Chiu P-C, Kuo Y-L, Tseng Y-H. Mechanism of Fe_2TiO_5 as oxygen carrier for chemical looping process and evaluation for hydrogen generation. Ceram Int. 2014;40(3):4599–605. doi:10.1016/j.ceramint.2013.08.138.
20. He F, Li X, Zhao K, Huang Z, Wei G, Li H. The use of $La_{1-x}Sr_xFeO_3$ perovskite-type oxides as oxygen carriers in chemical-looping reforming of methane. Fuel. 2013;108:465–73. doi:10.1016/j.fuel.2012.11.035.
21. Rydén M, Leion H, Mattisson T, Lyngfelt A. Combined oxides as oxygen-carrier material for chemical-looping with oxygen uncoupling. Appl Energy. 2014;113:1924–32. doi:10.1016/j.apenergy.2013.06.016.
22. de los Ríos Castillo T, Gutiérrez JS, Ortiz AL, Collins-Martínez V. Global kinetic evaluation during the reduction of CoWO 4 with methane for the production of hydrogen. Int J Hydrogen Energy. 2013;38(28):12519–26. doi:10.1016/j.ijhydene.2012.11.109.
23. Pishahang M, Bakken E, Stølen S, Larring Y, Thomas CI. Oxygen non-stoichiometry and redox thermodynamics of $LaMn_{1-x}CoxO_{3-\delta}$. Solid State Ionics. 2013;231:49–57. doi:10.1016/j.ssi.2012.10.009.
24. Matsushita Y, Oyama Y, Hasegawa M, Takei H. Growth and structural refinement of orthorhombic SrCuO2 crystals. J Solid State Chem. 1995;114(1):289–93. doi:10.1006/jssc.1995.1043.

25. Tanaka M, Hasegawa M, Takei H. Growth and anisotropic physical properties of SrCuO2 single crystals. Phys C. 1996;261(3–4):309–14. doi:10.1016/0921-4534(96)00176-1.
26. Ksepko E. Perovskite-type $Sr(Mn_{1-x}Ni_x)O3$ materials and their chemical-looping oxygen transfer properties. Int J Hydrogen Energy. 2014;39(15):8126–37. doi:10.1016/j.ijhydene.2014.03.093.
27. Clayton CK, Whitty KJ. Measurement and modeling of decomposition kinetics for copper oxide-based chemical looping with oxygen uncoupling. Appl Energy. 2014;116:416–23. doi:10.1016/j.apenergy.2013.10.032.
28. Adanez J, Abad A, Garcia-Labiano F, Gayan P, de Diego LF. Progress in chemical-looping combustion and reforming technologies. Prog Energy Combust Sci. 2012;38(2):215–82. doi:10.1016/j.pecs.2011.09.001.
29. Lippens BC, Linsen BG, de Boer JH. Studies on pore systems in catalysts I. The adsorption of nitrogen; apparatus and calculation. J Catal. 1964;3(1):32–7. doi:10.1016/0021-9517(64)90089-2.
30. de Boer JH, Linsen BG, Osinga TJ. Studies on pore systems in catalysts: VI. The universal t curve. J Catal. 1965;4(6):643–8. doi:10.1016/0021-9517(65)90263-0.